Research Square

Preprints are preliminary reports that have not undergone peer review.
They should not be considered conclusive, used to inform clinical practice,
or referenced by the media as validated information.

Proteome, volatile flavour and bacterial community shifts in Guanling yellow cattle beef during superchilled modified-atmosphere storage

Jiu-Ling Long
Guiyang University
Lu Lei
Guizhou Academy of Agricultural Sciences
Hao-Xiang Xu
Guizhou Academy of Agricultural Sciences
Wen-Ju Luo
Guizhou Academy of Agricultural Sciences
Weng-Kang Hu
Guizhou Academy of Agricultural Sciences
Yuan-Feng Zhao
Guizhou Academy of Agricultural Sciences
Qing-Feng Wang
Guizhou Academy of Agricultural Sciences
Rong Ai
Guizhou Academy of Agricultural Sciences
Ling-Ling Jiang
Guizhou Academy of Agricultural Sciences
Bo Yu
yubonky@163.com

Guizhou Academy of Agricultural Sciences

Research Article

Keywords: Guanling yellow cattle, superchilled storage, modified-atmosphere packaging, shelf-life, volatile organic compounds, 16S rRNA sequencing

Posted Date: November 23rd, 2026

DOI: https://doi.org/10.21203/rs.3.rs-11697150/v1

License: This work is licensed under a Creative Commons Attribution 4.0 International License.
Read Full License

Additional Declarations: No competing interests reported.

Proteome, volatile flavour and bacterial community shifts in Guanling yellow cattle beef during superchilled modified-atmosphere storage

Lu Lei 1, Jiu-Ling Long 2, Hao-Xiang Xu 1, Wen-Ju Luo 1, Weng-Kang Hu 1, Yuan-Feng Zhao 1, Qing-Feng Wang 1, Rong Ai 1, Ling-Ling Jiang 1, Bo Yu 1,*

1 Guizhou Institute of Animal Husbandry and Veterinary Sciences, Guizhou Academy of Agricultural Sciences, Guiyang, China

2 College of Food Science and Engineering, Guiyang University, Guiyang, China

* Correspondence: Bo Yu (Guizhou Institute of Animal Husbandry and Veterinary Sciences, Guizhou Academy of Agricultural Sciences, Guiyang, China). E-mail: （yubonky@163.com）

Abstract

Fresh beef from Guanling yellow cattle loses much of its value through a short shelf life, yet the molecular events that precede a conventional spoilage verdict are poorly described. We followed tenderloin packaged under 30% CO_2 / 20% O_2 / 50% N_2 at −1 °C for 14 d and measured the proteome, the volatile fraction and the bacterial community on aliquots of the same packages by DIA mass spectrometry, HS-SPME-GC-MS and 16S rRNA sequencing. Of 2,438 proteins quantified, 19, 23 and 27 changed in abundance over 0–7, 0–14 and 7–14 d; the later sets shifted from membrane trafficking and lipidation to intermediate-filament, integrin and extracellular-matrix proteins. Total volatile concentration fell from 751.2 to 535.7 ng/g in the first week and rose to 1,261.5 ng/g by day 14, when ketones, acids and nitrogen-containing compounds appeared alongside aldehydes. *Brochothrix* reached 30.8% of the community at 14 d. At that point TVB-N had passed the 15 mg/100 g limit while viable counts stayed below 5 log CFU/g and sensory scores remained acceptable, so the samples sat at the shelf-life boundary, short of overt spoilage. Volatiles tracked the bacterial community more closely than the proteome. We put forward propanal, 1-octen-3-ol and their associated taxa as candidates for monitoring quality loss during superchilled storage; they need validation in independent shelf-life trials.

Keywords: Guanling yellow cattle; superchilled storage; modified-atmosphere packaging; shelf-life; volatile organic compounds; 16S rRNA sequencing

1 Introduction

Guanling yellow cattle is a mountain breed raised in southwestern Guizhou. The animals grow slowly and the meat is lean, dark and well regarded locally for eating quality (Zhou et al., 2024). Almost all of it leaves the region as chilled carcass or primal cuts, so its value depends on how long it lasts in the cold chain. Fresh beef supports microbial growth and at the same time undergoes endogenous enzymatic and oxidative change; in practice the two are hard to disentangle. Discolouration, drip loss, toughening and off-odour tend to arrive together, and by the time a consignment is judged spoiled several mechanisms have already acted.

Superchilling (ice-temperature storage) and MAP are the two industrial answers to this problem. Holding meat just above its freezing point slows microbial growth and enzyme activity without the tissue damage caused by ice crystals. A CO_2-enriched atmosphere suppresses the growth of Gram-negative spoilage bacteria; O_2 is retained at a moderate level to keep myoglobin oxygenated, and N_2 fills the remaining

headspace (Feng et al., 2025; Yang et al., 2024). Neither technology is a simple antimicrobial switch. CO_2 solubility increases as temperature falls, so a gas mix that is adequate at 4 °C may be excessive or, after dissolution and package collapse, insufficient at −1 °C; and the O_2 included for colour is itself a substrate for lipid oxidation. The outcome therefore depends on gas composition, temperature, initial load and storage time acting together, which is why preservation trials report such inconsistent shelf lives for nominally similar treatments.

Proteomics has been used to describe what happens inside the tissue during this period. Studies on postmortem beef have linked changes in mitochondrial and glycolytic proteins to colour stability and to the onset of rigor (Ding et al., 2022; Krauskopf et al., 2025; Liu et al., 2022). Proteomic comparisons of packaging regimes have shown that high-O_2 MAP maintains an attractive cherry-red colour early on while accelerating oxidative stress and discolouration later (Krauskopf et al., 2025). Most of this work, however, ends with a list of differentially abundant proteins annotated to Gene Ontology terms (Lu et al., 2026). Relatively few studies follow a pathway through to a measurable quality attribute, and fewer still place the proteome alongside the two other layers that determine how beef actually smells and spoils.

Those layers are the volatile metabolome and the surface microbiota. Volatile flavour compounds in stored beef arise from lipid oxidation, amino acid and protein degradation, carbohydrate metabolism and bacterial metabolism, often simultaneously (Al-Dalali et al., 2022; Yu et al., 2025). Microbial succession under MAP has been characterised repeatedly. *Pseudomonas* dominates aerobically packaged meat, *Brochothrix thermosphacta* tolerates CO_2 and produces buttery, dairy-like off-odours, and lactic acid bacteria often prevail when CO_2 is high and O_2 low (Chen et al., 2025; Hou et al., 2023; Xu et al., 2024; Yang et al., 2022, 2025). The two layers are also coupled. 1-Octen-3-ol, for instance, is both a linoleate oxidation product and a metabolite of *B. thermosphacta* (Chen et al., 2025; Fang et al., 2022), so attributing a volatile to a source requires measuring both.

What is missing is an account that puts the three layers on the same samples and asks which of them tracks quality loss most closely. Omics integration has begun to be applied to spoilage ecology (Poirier et al., 2023), but usually to the microbial and chemical layers, rarely to the tissue proteome. Studies of Chinese indigenous breeds under superchilled MAP are particularly scarce, and the few available tend to report conventional indicators only (Zhou et al., 2024). We therefore designed a study with three destructive sampling points on a single packaging regime, applying DIA proteomics, HS-SPME-GC-MS and 16S rRNA sequencing to aliquots of the same packages. The same packaging regime was characterised in parallel by conventional quality indicators and a kinetic shelf-life model (Xu et al., 2027), which supplies the quality endpoint against which the molecular data are interpreted. Our working hypothesis was that endogenous protein change would dominate the early phase of storage and that microbial metabolism would take over as storage proceeded; the correlation structure among the three datasets was used to test this.

2 Materials and methods

2.1 Beef samples and packaging

Tenderloin (*psoas major*) was obtained from Guanling yellow cattle slaughtered at a commercial facility (Guizhou Yellow Cattle Industry Group Co., Ltd.) and transported to the laboratory within 2 h. On a sterile bench, surface fascia and visible fat were trimmed away and the muscle was cut into 50 × 50 × 15 mm blocks (40 ± 2 g). Two blocks were placed in each tray, which was then sealed under 30% CO_2 / 20% O_2 / 50% N_2 on a tray-sealing machine. Three independent packages were prepared for each sampling point and

stored at −1 °C in the dark. No package was opened before its designated sampling day, so the 0, 7 and 14 d samples (groups A, B and C; n = 3 each) are separate packages, not repeated openings of the same tray.

2.2 Determination of the ice-temperature point

The freezing point was determined from a cooling curve. A thermocouple was inserted into the geometric centre of a beef block, and core temperature was logged at 2-min intervals while the sample was cooled to below −10 °C. The plateau at which the rate of temperature decline abruptly slowed was taken as the freezing point (−1.1 °C); −1 °C was therefore used as the storage temperature, leaving a margin of 0.1 °C above the freezing point.

2.3 Conventional quality and microbiological analyses

Total viable counts (TVC) were determined on plate count agar following GB 4789.2-2022, and total volatile basic nitrogen (TVB-N) by the automated Kjeldahl method following GB 5009.228-2016. pH was measured with a portable penetration pH meter and colour (L*, a*, b*, D65 illuminant) with a colorimeter after 30 min of bloom. Sensory quality was scored by a 20-member panel of laboratory staff (10 male, 10 female), all screened and trained for the task, on a 10-point scale for appearance, odour and texture; the sensory score reported in Table 1 is the mean of these three attributes. All determinations, including the five-gas-composition comparison and the kinetic shelf-life model, were performed as described in the companion study on the same storage trial (Xu et al., 2027). Values for the 30% CO_2 / 20% O_2 / 50% N_2 regime at 0, 7 and 14 d are cited here as the quality endpoint for the molecular data.

2.4 Proteomics

2.4.1 Protein extraction and digestion

Samples were homogenised (FastPrep-24) in SDC lysis buffer (5% sodium deoxycholate, 100 mM Tris-HCl, pH 8.5), boiled for 15 min and centrifuged at 14,000 × g for 40 min. Supernatants were quantified by BCA assay. Aliquots containing 15 µg protein were reduced with DTT (37 °C, 1.5 h), alkylated with iodoacetamide (30 min at room temperature in the dark) and digested with trypsin at 1:50 (w/w) overnight at 37 °C. Peptides were desalted on an MCX cartridge, dried, redissolved in 0.1% formic acid, quantified at 280 nm and spiked with iRT peptides.

2.4.2 DIA-MS acquisition and data processing

Peptides were separated on a Vanquish Neo LC system and analysed on an Orbitrap Astral mass spectrometer operating in DIA mode (m/z 380–980; MS1 resolution 240,000; 299 MS2 isolation windows of 2 m/z; HCD collision energy 25 eV). Spectra were searched in DIA-NN 1.8.1 with trypsin/P specificity and one missed cleavage allowed; carbamidomethylation of cysteine was fixed, oxidation of methionine and N-terminal acetylation were variable, and the protein false discovery rate was set at 1%.

2.5 Volatile compounds

2.5.1 Extraction

A 3.0 g portion of minced beef was weighed into a 20 mL headspace vial with 1 µL of 2-methyl-3-heptanone (0.816 µg/µL) as internal standard, equilibrated at 50 °C for 20 min under magnetic stirring, and extracted for 40 min at 50 °C with a DVB/CAR/PDMS fibre (Supelco). The fibre was desorbed in the injection port at 250 °C for 5 min.

2.5.2 GC-MS conditions

Analysis used an Agilent 7890A-7000 GC-MS fitted with a DB-Wax column (60 m × 0.25 mm × 0.25 μm; J&W Scientific). Helium (>99.999%) was the carrier gas at 1.5 mL/min under splitless injection. The oven was held at 40 °C for 3 min, ramped to 250 °C at 4 °C/min and held for 5 min; the transfer line was kept at 250 °C. Mass spectra were acquired in EI mode (70 eV) with the ion source at 280 °C, scanning m/z 45–450.

2.5.3 Aroma-attribute profile

The nine-axis profile in Figure 5E was not generated by a sensory panel and is not a sensory measurement. It was produced by the commercial service provider that carried out the GC-MS work. Each identified volatile was assigned to the odour descriptor categories reported for it in the spectral library (sweet, bitter, pungent, fruity, floral, fresh, nutty, fatty, waxy), and the contribution of each category was expressed on a 0–120 relative scale. The profile is therefore a re-expression of the volatile composition, not independent evidence about perceived aroma. We treat it that way in section 3.3.

2.6 16S rRNA gene sequencing

2.6.1 DNA extraction and PCR

A 0.2–0.5 g portion was homogenised at 60 Hz (Tissuelyser-48, Shanghai Jingxin) in lysis buffer, and total DNA was extracted with the OMEGA Soil DNA Kit (D5635-02), checked on 0.8% agarose gels and quantified on a NanoDrop NC2000. The V3–V4 region (~468 bp) was amplified with primers 338F (5′-barcode-ACTCCTACGGGAGGCAGCA-3′) and 806R (5′-GGACTACHVGGGTWTCTAAT-3′). Each 25 μL reaction contained 0.25 μL Q5 high-fidelity polymerase, 5 μL 5× reaction buffer, 5 μL 5× High GC buffer, 2 μL dNTPs (10 mM), 2 μL template DNA, 1 μL of each primer (10 μM) and 8.75 μL water. Cycling was 98 °C for 5 min; 25 cycles of 98 °C 30 s, 53 °C 30 s, 72 °C 45 s; and 72 °C for 5 min. Products were purified from 2% agarose gels (Axygen).

2.6.2 Library preparation and sequencing

Purified products were quantified (PicoGreen, BioTek FLx800) and pooled. Libraries were prepared with the TruSeq Nano DNA LT Kit: 30 ng DNA was end-repaired (30 °C, 30 min), purified with AMPure XP, A-tailed (37 °C 30 min, 70 °C 5 min), ligated to adapters (30 °C, 10 min), amplified and size-selected on 2% agarose gels. Libraries showing a single peak without adapter contamination and a concentration ≥2 nM were checked on a Bioanalyzer 2100, pooled, denatured with 0.1 N NaOH and sequenced (2 × 250 bp) on an Illumina NovaSeq 6000 at 15–18 pM.

2.7 Data analysis

Proteomic data were processed in R 4.2.0. Hierarchical clustering, PCA and OPLS-DA were used to describe sample structure, and the OPLS-DA model was described by R^2X, R^2Y and Q^2. Proteins were annotated against GO with Blast2GO; enrichment used Fisher's exact test with Benjamini–Hochberg correction, and GSEA was run on the ranked protein list (Subramanian et al., 2005). Subcellular localisation and domain annotation used CELLO and InterProScan, and protein–protein interactions were retrieved from STRING. Volatiles were identified against the NIST library and confirmed by retention index, and semi-quantified against the 2-methyl-3-heptanone internal standard. Odour activity values (OAV) were calculated as concentration divided by the published odour threshold in water or oil, with the source of each threshold given in Table S1.

16S rRNA reads were processed in QIIME2 with DADA2, and taxonomy was assigned against Greengenes; alpha diversity indices were compared by Kruskal–Wallis test, beta diversity used Bray–Curtis distances with NMDS ordination and PERMANOVA, and metabolic function was predicted with PICRUSt2. Associations among protein, volatile and genus matrices were assessed by Pearson correlation and Mantel tests. These analyses used the 0 d and 14 d samples only (n = 6). The volatile profile changed non-monotonically over the trial, falling at 7 d before a second accumulation (section 3.3), so an endpoint comparison kept the direction of each association unambiguous. The 7 d samples were reserved for the proteomic and community analyses, which changed monotonically. Because the correlations rest on six samples drawn from a single trajectory, their p-values are reported unadjusted and the results are read descriptively (section 4.4); the Benjamini–Hochberg procedure was applied to the protein and volatile comparisons, where significance was set at adjusted $p < 0.05$.

3 Results

3.1 Conventional quality indicators and the shelf-life endpoint

The storage trial was characterised in parallel by conventional quality analyses (Xu et al., 2027); the values for the 30% CO_2 / 20% O_2 / 50% N_2 regime are summarised in Table 1 and anchor the molecular data to a measurable quality trajectory.

Total viable counts rose from 3.00 log CFU/g at 0 d to 3.53 log CFU/g at 7 d and 4.90 log CFU/g at 14 d, gaining 0.5 log over the first week and 1.4 log over the second. They stayed below the 6 log CFU/g conventionally taken as the threshold for microbiological spoilage. TVB-N behaved differently. From 10.38 mg/100 g at 0 d it reached 13.53 mg/100 g at 7 d and 16.29 mg/100 g at 14 d, so the 15 mg/100 g limit (GB 2707) was crossed between days 7 and 14. A kinetic model fitted to the same trial predicted a shelf life of 13.6 d at −1 °C with TVB-N as the limiting indicator, and linear interpolation of the measured values gave 14.1 d (Xu et al., 2027). Sensory scores declined in step, from 8.80 to 7.53 and 6.53, and remained at the lower edge of acceptability at the end of storage.

pH and colour moved far less. pH was essentially unchanged over the first week (6.00 to 5.90) and fell to 5.50 by day 14, staying between 5.5 and 6.0 throughout. It never showed the late rise that accompanies ammonia accumulation in air-stored beef; dissolved CO_2 holds the tissue below the point where that rise begins. L* stayed within one unit of its initial 30.45 (31.16 at 7 d, 29.60 at 14 d), and a* fell from 21.59 to 20.44 at 7 d and to 16.71 at 14 d. Redness therefore faded gradually, with no abrupt discoloration at the point where the volatile profile turned.

These indicators place the 14 d samples at the end of the predicted shelf life. The nitrogen fraction had passed the regulatory limit, while counts and sensory scores show that overt microbiological spoilage had not arrived. The molecular data below therefore describe tissue on the way into spoilage, before spoilage is detectable. That timing is what would make markers extracted from them useful as early warnings.

3.2 Proteome

3.2.1 Identification

A total of 2,438 proteins were quantified across the nine samples. Mean protein numbers in groups A, B and C were 2,333.3, 2,320.7 and 2,296.7, with corresponding mean peptide numbers of 23,166, 22,749 and 22,433 (Figure 1A). The decline from 0 to 14 d amounted to less than 2% of the protein count, which fits

limited proteolysis, not wholesale degradation. About 90% of the identified peptides were 6–18 amino acids long (Figure 1B), so digestion and identification were consistent across the nine samples. Of the 2,438 proteins, 2,282 were shared by all three groups, and 22, 13 and 7 were unique to A, B and C (Figure 1C). Storage changed the abundance of a common protein set without reshaping its composition.

3.2.2 Sample structure

PCA separated the three groups along PC1 and PC2 with tight within-group clustering (Figure 2A). A supervised OPLS-DA model separated them completely, with $R^2X = 0.915$, $R^2Y = 0.982$ and $Q^2 = 0.973$ (Figure 2B). We note that these values were obtained with nine samples and a large variable set, and interpret the separation as descriptive of group structure, not evidence of predictive biomarker performance.

3.2.3 Differentially abundant proteins

With fold change > 1.5 and $p < 0.05$ as criteria, 19, 23 and 27 proteins differed in abundance in A vs B, A vs C and B vs C, respectively (Figure 3A). The largest number of changes therefore fell in the 7–14 d interval.

Between 0 and 7 d, 11 proteins were more abundant at 0 d and 8 at 7 d (Figure 3B). Those higher at 7 d included AVPR2, GGCT, F13A1, HSBP1, EPN1, COL6A6 and NMT1. The combination matters more than the individual names. NMT1 and the accompanying enrichment of myristoyltransferase activity indicate N-myristoylation, GGCT points to glutathione cycling and HSBP1 to heat-shock regulation, and all three fit a tissue readjusting membrane anchoring and redox buffering as cold and CO_2 begin to take effect. The changes themselves were small, as expected from a system under stress that has not yet lost structure.

The 0–14 d comparison yielded 23 DAPs (Figure 3C). Proteins higher at 14 d included GBA1, AKR1C4, XPO7, ARF6, CASTOR2, UBA6, ILVBL, PPM1F, G3BP1 and EPN1. Three indicate what kind of change this is: GBA1 points to lysosomal glycosphingolipid catabolism, AKR1C4 to aldo-keto reduction and redox handling, and UBA6 to ubiquitin-dependent turnover. Six proteins moved the other way: FRMD3, AKAP1, ITIH5, THBS4, ITGA7 and STAT3. This is the more informative half of the comparison. ITGA7 and THBS4 belong to the integrin–extracellular matrix axis, and their decline points to loosening of cell–matrix adhesion. AKAP1, a mitochondrial scaffold protein, also fell, in line with the loss of mitochondrial integrity discussed below.

The 7–14 d window contained the greatest number of changes, 27 (Figure 3D). Proteins rising at 14 d included SARS2, FECH, ACTA1, NDUFV3, JSRP1, UBA6, PSMG2, COX6A2 and AKR1C4, spanning mitochondrial translation (SARS2), haem synthesis (FECH), respiratory-chain subunits (NDUFV3, COX6A2) and proteasome assembly (PSMG2). Proteins that were higher at 7 d than at 14 d included the keratins KRT5 and KRT75, DCTN4, ITGA7, ITIH5, NMT1 and STAT3, i.e. intermediate-filament and cytoskeletal-anchoring components. Across the two later comparisons the dominant signal moves from metabolic and redox regulation to structural proteins. That is the point at which the tissue stops adjusting and starts coming apart.

3.2.4 Functional enrichment and GSEA

GO and KEGG enrichment for the A vs C comparison is shown in Figure 4A–C. The biological-process terms (Figure 4A) cover protein acylation, lipidation and targeting to membrane, alongside cell–substrate junction organisation; the cellular-component terms (Figure 4B) include intermediate filament and focal adhesion; and KEGG (Figure 4C) returns focal adhesion, PI3K–Akt signalling, ECM–receptor interaction, oxidative phosphorylation and sphingolipid metabolism. The terms also shift over time in the same direction

as the proteins. Lipidation and membrane trafficking dominate the 0–7 d set, sphingolipid and junction terms the 0–14 d set, and intermediate-filament and integrin signalling the 7–14 d set (Shu et al., 2025; Yuan et al., 2024).

GSEA ranks the whole proteome, not a filtered subset. It returned significant enrichment for oxidative phosphorylation (NES −2.56, FDR 8.97×10^{-8}) and respiratory electron transport (NES −2.44, FDR 1.47×10^{-6}) (Figure 4D, E), in line with earlier work on mitochondrial proteins in chilled beef (Liu et al., 2022; Luo et al., 2021). The direction needs care. Mitochondrial function falls in excised tissue, so a change in the abundance of respiratory-chain subunits reflects redistribution and degradation as much as any change in respiratory capacity (Ding et al., 2022).

3.3 Volatile compounds

3.3.1 Composition

Seventy-one volatiles were detected across the three groups, 33 of them shared; 7, 1 and 6 were unique to A, B and C (Figure 5A). Total concentration changed sharply with storage time: 751.2 ± 5.1 ng/g at 0 d, 535.7 ± 25.2 ng/g at 7 d and 1,261.5 ± 31.5 ng/g at 14 d. The 14 d value was 1.68 times the 0 d value and 2.35 times the 7 d value (Figure 5B). The dip at 7 d is unlikely to be an analytical artefact. The headspace at that point was carried by a few abundant alcohols. That is not the same thing as a weaker smell.

The class composition explains the trajectory (Figure 5C, D). Group A was aldehyde-dominated (406.8 ng/g, 54.2%) with a substantial sulfur fraction (187.4 ng/g, 25.0%), the signature of ongoing lipid cleavage plus low-threshold sulfur volatiles. In group B alcohols took over (299.5 ng/g, 55.9%), with aldehydes down to 136.2 ng/g (25.4%), the expected consequence of aldehyde reduction to alcohols once the primary oxidation burst had passed. Group C returned to aldehyde dominance (638.4 ng/g, 50.6%) but now with alcohols at 190.2 ng/g, ketones at 142.1 ng/g and, for the first time, measurable acids and nitrogen-containing compounds. That combination is not simply a later stage of the same process; it indicates that a second, microbially driven set of reactions had started.

The aroma-attribute profile sorts the groups in the same sequence (Figure 5E). Sweet and waxy descriptors dominate group A, floral and fatty ones group B, and pungent, fruity and bitter ones group C. This follows from the compounds listed above (propanal and phenylacetaldehyde in A, the alcohol shift in B, pentanoic acid and indole in C), so the profile restates the class-level composition in perceptual terms without confirming it independently.

3.3.2 Compounds that dominated each stage

Group A was dominated by propanal (279.6 ng/g), dimethyl trisulfide (186.2 ng/g) and phenylacetaldehyde (102.4 ng/g) (Figure 6A). Propanal is a classical autoxidation product of n-3/n-6 polyunsaturated fatty acids and carries a mild, fatty note; phenylacetaldehyde, formed by Strecker degradation of phenylalanine, contributes a honey-like sweetness. Dimethyl trisulfide was present at lower concentration but has an odour threshold in the low ng/g range, so its sulfury, cabbage-like note probably shapes the aroma of fresh beef far more than its share of the total suggests (Yu et al., 2025).

Group B was led by 1-undecanol (139.3 ng/g) followed by 1-octen-3-ol (70.3 ng/g), propanal and (Z)-9-octadecen-1-ol (Figure 6B). 1-Octen-3-ol rose at 7 d. It is a linoleate hydroperoxide cleavage product with a mushroom, earthy note, and *B. thermosphacta* makes it as well, so its appearance marks the point where oxidative and microbial routes become hard to separate.

Group C showed simultaneous elevation of aldehydes, ketones, acids and nitrogen-containing compounds (Figure 6C), the volatile signature of amino acid catabolism superimposed on continued lipid oxidation.

3.3.3 Differential volatiles

One-way ANOVA identified 11 volatiles that differed among groups ($p < 0.05$), and hierarchical clustering separated 0 d from the two later groups, with B and C clustering together (Figure 7). Acrolein was highest at 0 d and declined thereafter, which is plausible for a reactive α,β-unsaturated aldehyde consumed by further oxidation or by addition to amino groups (Al-Dalali et al., 2022). Group B was marked by 1-octen-3-ol, propanal, 2-nonanone and ethyl palmitate; group C by pyridine, benzene, phenylethyl alcohol, propanoic anhydride, 2-undecanone and (Z)-9-octadecen-1-ol. Phenylethyl alcohol, formed from phenylalanine, is associated with *Pseudomonas* and *B. thermosphacta* activity in stored meat (Fang et al., 2022), and its appearance at 14 d coincides with the rebound of *Pseudomonas* described below.

3.4 Bacterial community

3.4.1 Alpha diversity

Sequence lengths clustered between 400 and 425 bp with a single peak near 420 bp (Figure 8), indicating consistent amplicon size selection. Chao1, observed species, Shannon, Pielou's evenness and Faith's PD were all highest at 0 d and declined at 7 and 14 d, while Simpson increased (Figure 9), so the community became poorer and more uneven as storage proceeded. None of these differences reached statistical significance ($p > 0.05$), and we report them as a consistent trend, not a demonstrated effect; with three samples per group the test has little power to detect the moderate shifts typically seen over 14 d.

3.4.2 Beta diversity

NMDS on Bray–Curtis distances separated the three groups (stress < 0.2) (Figure 10). Group A samples sat in the negative NMDS1 region with little internal scatter; B and C moved progressively along NMDS1 and became more dispersed, so that between-sample heterogeneity increased as the community reorganised. This is the pattern expected when a small number of taxa take over and their relative share depends on stochastic differences in initial load.

3.4.3 Community composition

At the phylum level (Figure 11A), group A was dominated by Proteobacteria (64.2%), with Actinobacteriota at 24.3% and Firmicutes at 9.2%. By 7 d Proteobacteria had fallen to 22.9% while Actinobacteriota and Firmicutes rose to 37.9% and 31.4%. At 14 d Firmicutes reached 42.1%, Proteobacteria recovered to 36.1%, Actinobacteriota dropped to 10.9% and Bacteroidota accumulated to 10.1%. The rise of Actinobacteriota to 37.9% at 7 d and its fall to 10.9% at 14 d tracks the trajectory of *Kocuria* and is taken up in section 4.3.

At the genus level (Figure 11B) the initial community was dispersed: *Acinetobacter* 16.7%, *Pseudomonas* 10.3%, *Corynebacterium* 10.3%. At 7 d, *Kocuria* reached its maximum (28.2%) and *Brochothrix* rose to 22.6%, while *Acinetobacter*, *Corynebacterium*, *Enterobacter* and *Psychrobacter* all declined. By 14 d *Brochothrix* was the single most abundant genus at 30.8%, *Pseudomonas* had returned to 18.9%, *Prevotella* appeared at 4.3% and *Kocuria* had fallen to 2.8%.

These numbers describe a two-stage succession: CO_2 displaced the initial Gram-negative aerobes, *Brochothrix* then consolidated, and *Pseudomonas* returned late. The intermediate peak of *Kocuria* is harder

to account for. It is a Gram-positive halotolerant coccus and not a typical meat spoilage organism, so we treat it with caution (section 4.3).

3.5 Associations across the three layers

Twelve DAPs were carried into this analysis, namely those that differed in at least two of the three pairwise comparisons (Table S2). Their correlation with the 11 differential volatiles gave a clear bipolar structure (Figure 12A). Five of them (GBA1, EPN1, ARF6, G3BP1, ILVBL) correlated positively with nine of the eleven volatiles and weakly negatively with acrolein and (Z)-9-octadecen-1-ol. The other seven (EIF3M, FRMD3, C10orf71, MBNL1, ITGA7, AKAP1, OSGEP) gave the mirror image. The split follows the two routes by which these volatiles arise, lipid oxidation and proteolysis, which is suggestive but no more: we treat the pattern as hypothesis-generating.

The protein–genus matrix gave the same split (Figure 12B). The five proteins more abundant at 14 d (GBA1, EPN1, ARF6, G3BP1 and ILVBL) correlated positively with the genera that rose over the same interval, and the seven that declined (EIF3M, FRMD3, C10orf71, MBNL1, ITGA7, AKAP1 and OSGEP) correlated negatively with them. The split is identical to that in Figure 12A, and the identity is the informative part. Because each variable was measured on the same two dates, the three matrices are dominated by storage time and are close to rank one, so the sign of a cell follows from whether its two variables rose or fell between 0 and 14 d. The three matrices in Figure 12A–C therefore describe a shared trajectory; they are not independent evidence that one layer drives another. The coefficients are also unstable at $n = 6$, where $|r| = 0.81$ corresponds to $p = 0.05$ and $|r| = 0.97$ to $p = 0.001$. Within-group variation is small next to the between-group change, so 94 of the 362 cells clear the $p < 0.001$ bar and the stars carry less information than their number suggests.

The volatile–genus matrix was tighter (Figure 12C). Five volatiles (2-nonanone, propanoic anhydride, propanal, phenylethyl alcohol and 1-octen-3-ol) correlated positively with most genera, and *Kocuria* was the exception, correlating negatively with all five. *Kocuria* also peaked and then collapsed while these volatiles rose, so a negative sign is what competitive displacement would give and not a direct metabolic role.

Mantel tests summarised this at the matrix level (Figure 12D). The volatile–protein and volatile–genus links were both significant; the second was the stronger and included the VOC–GBA1, VOC–ARF6, VOC–AKAP1 and VOC–ILVBL pairs at $p < 0.01$, whereas protein–protein links were mostly non-significant. Our interpretation leans on the ordering volatile–microbe > volatile–protein, with the caveat set out in section 4.4: what Mantel ranks is how tightly each layer follows the shared trajectory, not an isolated causal link between two layers. As a partial check we recomputed the correlations after removing the difference between the two sampling dates from each variable. The volatile–genus matrix kept more strong links than the protein–genus matrix, five pairs against two, among them 2-nonanone with *Brochothrix* and benzene with *Corynebacterium* at $|\text{partial } r| \geq 0.88$. With three residual degrees of freedom this comparison is suggestive only, but its direction agrees with the Mantel ordering.

4 Discussion

4.1 The proteome moves from regulation to structural failure

The DAP sets from the three comparisons are not simply cumulative; they describe a change in what the tissue is doing. Between 0 and 7 d the enriched terms (protein acylation, N-myristoylation, protein targeting

to membrane, protein export) all concern the routing of proteins between compartments. N-myristoylation in particular is a co-translational modification that decides whether a protein can associate with a membrane, and its enrichment, together with the rise in NMT1, implies that the cell was still actively re-addressing its membrane proteome at 7 d. The same reading applies to GGCT and glutathione cycling: early storage under elevated CO_2 is an oxidative and acidifying challenge, and the tissue buffers instead of breaking down. Myristoylation is one strand of a broader post-translational landscape that shifts around rigor, alongside phosphorylation, acetylation, ubiquitination and S-nitrosylation (Ren et al., 2025).

By 14 d this had changed. The dominant signals became intermediate-filament proteins (KRT5, KRT75), integrin α7, thrombospondin-4, ITIH5 and focal adhesion, with PI3K–Akt and ECM–receptor interaction appearing among the enriched pathways. These proteins hold the sarcolemma to the basal lamina and the basal lamina to the endomysium. When they are lost, the cytoskeleton detaches from the sarcolemma, membrane integrity fails, and the result is increased drip loss and the diffuse, pale appearance of over-stored beef (He et al., 2025; Zhu et al., 2021). Protein oxidation under elevated O_2 has itself been linked to calpain activation and accelerated desmin breakdown in MAP beef (Fu et al., 2017), which is the same direction of change seen here. The parallel decline in AKAP1 and the GSEA signal for oxidative phosphorylation fit the same story from the mitochondrial side, because mitochondrial scaffolding proteins are among the first casualties of permeability transition. The proteome therefore does not show the cause of spoilage. It shows the tissue losing the structural organisation on which spoilage proceeds.

One caveat shapes how these data can be used. Only 19–27 proteins out of 2,438 met the fold-change and p-value criteria. Muscle proteomes quantified by DIA are dominated by a few hundred abundant glycolytic and myofibrillar proteins, and the dynamic range compresses the apparent fold-change of low-abundance regulatory proteins. A short list is therefore expected in a study of this size, and it should not be read as evidence that little changed. Quantitatively the largest changes were in structural proteins, which is why the late-stage signal is the clearest part of the dataset.

4.2 Two oxidation waves, only one of them abiotic

The volatile data resolve into three stages, not a monotonic rise. Total concentration fell at 7 d before climbing steeply at 14 d, and the class composition explains why. The aldehyde pool produced by early lipid cleavage was partly reduced to alcohols, and alcohols have both higher odour thresholds and, in this system, a lower total mass contribution than the aldehyde burst they replaced. The 7 d dip is a chemical stage, not a measurement artefact, and a design that sampled only 0 and 14 d would miss it.

The second wave, from 7 to 14 d, is qualitatively different. Aldehydes return, but they are now accompanied by ketones, short-chain acids, pyridine, indole and phenylethyl alcohol. Methyl ketones such as 2-nonanone and 2-undecanone arise from β-oxidation of free fatty acids followed by decarboxylation, a route that requires lipase activity and points to microbial metabolism, not purely chemical oxidation. Pyridine and indole are products of amino acid catabolism; phenylethyl alcohol comes from phenylalanine. Their simultaneous appearance is the chemical signature of a community that has begun to ferment amino acids (Han et al., 2025), and it falls in the same interval as the consolidation of *Brochothrix* and the return of *Pseudomonas*. The conventional freshness data agree. TVB-N, the standard index of microbial protein degradation, crossed the 15 mg/100 g regulatory limit between 7 and 14 d in this regime (Table 1), which is the interval in which the methyl ketones, acids and nitrogenous volatiles appeared. Cadaverine, another amine formed by decarboxylation of free amino acids in the pack, has been proposed as a spoilage indicator in MAP beef for the same reason (Thamsborg et al., 2023). The companion analysis identified TVB-N as

the shelf-life-limiting indicator at −1 °C (Xu et al., 2027). That is consistent with the correlation structure reported here: the volatile profile tracked the bacterial community more closely than the proteome, and the attribute that limits shelf life is itself microbially driven.

Among the individual compounds, two stand out as trajectory markers. Propanal was present at high concentration from the start, declined as it was reduced or consumed, and rose again with the second wave, so that it tracks the overall oxidative load, not any single source. 1-octen-3-ol behaved differently: it was low at 0 d, peaked at 7 d and stayed high, and it has the unusual property of being formed both by linoleate hydroperoxide cleavage and by *B. thermosphacta* metabolism (Chen et al., 2025; Fang et al., 2022). That dual origin makes it a good indicator of the handover between oxidative and microbial spoilage, but a poor tool for attributing spoilage to one of them. Its odour threshold is low enough (approximately 1 ng/g in water) that the concentrations measured here would give OAVs in the tens; the same calculation for propanal and for dimethyl trisulfide, and the full OAV table, are given in Table S1.

4.3 CO_2 selection, and what the Kocuria peak means

The phylum-level pattern, with Proteobacteria collapsing at 7 d, Firmicutes rising and Proteobacteria partly recovering at 14 d, is what CO_2 dissolved in the aqueous phase of muscle would be expected to produce. CO_2 is more soluble at −1 °C than at 4 °C, so the effective inhibitory concentration in these packs was probably higher than the nominal 30% suggests. The initial Gram-negative aerobes (*Acinetobacter*, *Pseudomonas*, *Enterobacter*, *Psychrobacter*) were the taxa least able to cope (Hou et al., 2023; Yang et al., 2022). The subsequent return of Proteobacteria, driven by *Pseudomonas*, is the part that needs explaining. Two possibilities seem plausible to us: either the O_2 retained for colour maintenance allowed a CO_2-tolerant subpopulation of *Pseudomonas* to grow once competition had been removed, or the packages lost CO_2 through the lidding film over 14 d and the selective pressure weakened. Distinguishing between them would require headspace gas measurements at each sampling point, which we did not make; both remain hypotheses.

Absolute counts give this succession a firmer footing than relative abundance alone can provide. TVC rose from 3.00 to 4.90 log CFU/g over the trial, so the growing share of *Brochothrix* reflects real growth and not merely displacement of competitors. Counts nevertheless stayed below the level conventionally taken as spoilage, which agrees with the volatile data: the community was reorganising before any conventional spoilage verdict was reached.

The *Kocuria* result is the one we trust least. A Gram-positive, halotolerant coccus reaching 28.2% of the community at 7 d and then falling to 2.8% is not a pattern reported for MAP beef, and *Kocuria* is not a recognised spoilage organism. Three explanations are possible. It may have been a transient member of the initial flora that briefly benefited when competitors were removed, or it may have been introduced during handling and grown before CO_2 fully dissolved. The third is misassignment: *Kocuria* and related Micrococcaceae are close enough to other Actinobacteriota in the V3–V4 region that genus-level classification can be ambiguous. We flag the third as the most likely and would recommend re-checking these reads against a second reference database before the result is used. The same caution applies to *Prevotella* at 4.3% on day 14: it is a strict anaerobe of rumen origin, and a signal of that size in a 20% O_2 package points to carcass contamination or classification error, not growth.

Reading growth from those percentages assumes that TVC and the sequencing libraries describe the same bacterial load. Within the sequencing data alone, relative abundance cannot separate growth from displacement, so the genus-level percentages are shares of the community and nothing more. The absence

of a significant alpha-diversity effect at three samples per group also means the diversity trend belongs to the literature, not to the findings of this study (Yang et al., 2022; Wang et al., 2025).

4.4 Why the microbial layer tracks flavour more closely than the proteome

The Mantel results order the three matrices in a way that is biologically coherent. Volatile profiles covaried most strongly with the bacterial community, less strongly with the proteome, and the proteins covaried weakly among themselves. If protein abundance were driving flavour formation the opposite would be expected: coherent protein modules linking to coherent volatile groups. Instead the proteins respond to storage stress largely as individuals, consistent with the small number of DAPs shared between comparisons, while the volatile profile follows the community.

This does not mean the proteome is irrelevant to quality. The structural proteins that decline late are the ones that determine water-holding capacity and texture, and their loss is a quality outcome in its own right; it simply is not an aroma outcome. Our reading is that the two layers report on different quality attributes: the proteome reports on the physical deterioration of the tissue, and the microbiota on the chemical deterioration of its flavour. That division is more useful for preservation strategy than a single "spoilage mechanism". Interventions aimed at CO_2-tolerant organisms would buy aroma stability, whereas texture and drip loss depend on keeping structural integrity, which in practice means temperature control and limits on oxidative damage.

The interpretation has an obvious limit. Restricting the correlation analysis to the two endpoints was deliberate: it asks which layers changed together between the fresh and the end-of-shelf-life states. It also discards the intermediate time point and, with six samples spanning a single trajectory, cannot separate causation from co-variation with storage time. Within the two endpoints used here, nearly every variable rises or falls between 0 and 14 d, so any two of them will correlate. The Mantel test compares matrices, not individual pairs, which mitigates but does not remove the problem. A stronger design would decouple microbial growth from storage time, for instance with an irradiated or antibiotic-treated series. That is the next step we would take.

4.5 Limitations

The conventional indicators that anchor the omics interpretation (TVC, pH, TVB-N, colour, sensory score) come from a companion study on the same trial (Xu et al., 2027). They were not independently replicated here, and texture and drip loss were not measured at all. The omics trial also contained no packaging control. The comparison across gas compositions that motivates the MAP context belongs to the companion study, so what we report describes this regime, not its effect relative to other atmospheres. Each sampling point rests on three independent packages, enough for consistent trends but underpowered for the modest effects typical of alpha diversity and of low-abundance proteins. The correlations inherit that weakness. One muscle, one breed and one farm were sampled, so extrapolation to other cuts and production systems is not warranted.

5 Conclusions

Over 14 d at −1 °C under 30% CO_2 / 20% O_2 / 50% N_2, Guanling yellow cattle tenderloin moved to the boundary of its predicted shelf life. TVB-N crossed the regulatory limit between days 7 and 14, while bacterial counts stayed below 5 log CFU/g and the samples remained sensorily acceptable. Over the same interval the tissue passed through three distinguishable molecular states. Protein changes were modest in

number but shifted in character, from membrane trafficking and redox regulation at 7 d to intermediate-filament, integrin and extracellular-matrix proteins at 14 d, a transition from adjustment to structural loss. Volatiles followed a two-wave pattern, with an aldehyde-to-alcohol shift at 7 d and a second, microbially driven accumulation of aldehydes, methyl ketones, acids and nitrogenous compounds at 14 d. The bacterial community moved from a diverse Gram-negative assemblage to one dominated by *Brochothrix* (30.8% at 14 d), with *Pseudomonas* returning late.

The volatile–microbe association was stronger than the volatile–protein association, and TVB-N was the shelf-life-limiting indicator in the companion study. Together these suggest that microbial metabolism paces aroma deterioration in this system, while the proteome records structural decline. In practice that points to CO_2-tolerant organisms as the target for aroma stability, and to temperature and oxidative control as the route to texture and water-holding capacity. Combining packaging and temperature hurdles with knowledge of where the meat came from is the practical form of that argument (Li et al., 2025). The markers identified here (propanal, 1-octen-3-ol and their associated taxa) changed at the shelf-life boundary while bacterial counts were still low, which is the property expected of early-warning signals. They now need to be validated against sensory rejection and plate counts in independent trials before operational use.

Declarations

Ethics approval and consent to participate

Animals were slaughtered at a licensed commercial abattoir under routine veterinary inspection, and the muscle used in this study was obtained post-mortem as a commercial product. No live animals were used and no experimental procedures were applied to animals; ethical approval for animal experimentation was therefore not required. The sensory panel consisted of laboratory staff who took part voluntarily, were informed of the nature of the samples and the scoring procedure, and gave informed consent before evaluation. No personally identifiable information was collected.

Consent for publication

Not applicable.

Availability of data and materials

The 16S rRNA sequence data and the DIA mass spectrometry proteomics data generated in this study will be deposited in the NCBI Sequence Read Archive and in the ProteomeXchange Consortium via the iProX partner repository, respectively; accession numbers will be added before publication. The conventional quality and shelf-life data (TVC, pH, TVB-N, colour, sensory) are reported in a companion study (Xu et al., 2027). All other datasets supporting the conclusions of this article are available from the corresponding author on reasonable request.

Competing interests

The authors declare that they have no competing interests.

Funding

This work was supported by the Youth Guidance Project of the Guizhou Provincial Basic Research Program (QKHJC-QN[2025]-235), the Youth Fund of the Guizhou Academy of Agricultural Sciences (QNKYBJJ-[2025]-13), the Innovative Research Groups Program of the Guizhou Academy of Agricultural Sciences

(2026-12), and the Guizhou Provincial Key Laboratory of Livestock and Poultry Genetic Resources Innovation and Utilization (ZSYS[2025]034).

Authors' contributions

Lu Lei: methodology, data curation, formal analysis, visualisation, writing – original draft. Jiu-Ling Long: investigation, resources, writing – review and editing. Hao-Xiang Xu: conceptualisation, project administration, resources. Wen-Ju Luo: validation. Weng-Kang Hu: investigation. Yuan-Feng Zhao: supervision. Qing-Feng Wang: visualisation. Rong Ai: validation. Ling-Ling Jiang: supervision. Bo Yu: supervision, project administration.

References

Al-Dalali, S., Li, C., & Xu, B. (2022). Insight into the effect of frozen storage on the changes in volatile aldehydes and alcohols of marinated roasted beef meat: potential mechanisms of their formation. *Food Chemistry, 385*, 132629. https://doi.org/10.1016/j.foodchem.2022.132629

Chen, L., Ryu, R., Kuuliala, L., Somrani, M., Walgraeve, C., Demeestere, K., & Devlieghere, F. (2025). Modeling the growth and volatile metabolite production of spoilage-causing *Brochothrix thermosphacta* on solid meat substrates under modified atmospheres. *International Journal of Food Microbiology, 434*, 111150. https://doi.org/10.1016/j.ijfoodmicro.2025.111150

Ding, Z., Wei, Q., Liu, C., Zhang, H., & Huang, F. (2022). The quality changes and proteomic analysis of cattle muscle postmortem during rigor mortis. *Foods, 11*(2), 217. https://doi.org/10.3390/foods11020217

Fang, J., Feng, L., Lu, H., & Zhu, J. (2022). Metabolomics reveals spoilage characteristics and interaction of *Pseudomonas lundensis* and *Brochothrix thermosphacta* in refrigerated beef. *Food Research International, 156*, 111139. https://doi.org/10.1016/j.foodres.2022.111139

Feng, C., Sun, K., Zhang, Y., Liang, R., Mao, Y., Hopkins, D.L., Zhu, L., Luo, X., & Yang, X. (2025). Differentiated application of oxygen levels for the preservation of high-oxygen packaged beef based on initial microbial contamination. *Meat Science, 225*, 109803. https://doi.org/10.1016/j.meatsci.2025.109803

Fu, Q., Ge, Q., Liu, R., Wang, H., Zhou, G., & Zhang, W. (2017). Influence of modified atmosphere packaging on protein oxidation, calpain activation and desmin degradation of beef muscles. *Journal of the Science of Food and Agriculture, 97*(13), 4508–4514. https://doi.org/10.1002/jsfa.8316

Han, M., Gu, Q., Al-Dalali, S., Chen, C., Xu, B., & Li, P. (2025). Changes in volatile organic compounds of tray-packed fresh beef sausages under refrigeration: the roles of dominant spoilage bacteria. *Meat Science, 229*, 109914. https://doi.org/10.1016/j.meatsci.2025.109914

He, W., Peng, Y., Huang, H., Hang, L., Liu, Z., Yu, H., & Zhang, Y. (2025). Postmortem changes of desmin, talin-2, vinculin, and integrin β1 in chicken breast and their effects on tenderness. *Journal of Agricultural and Food Chemistry, 73*(12), 7393–7404. https://doi.org/10.1021/acs.jafc.4c13003

Hou, X., Zhao, H., Yan, L., Li, S., Chen, X., & Fan, J. (2023). Effect of CO_2 on the preservation effectiveness of chilled fresh boneless beef knuckle in modified atmosphere packaging and microbial diversity analysis. *LWT, 187*, 115262. https://doi.org/10.1016/j.lwt.2023.115262

Krauskopf, M.M., Antonelo, D.S., de Araújo, C.D.L., Balieiro, J.C.C., Delgado, E.F., Ramanathan, R., & Contreras Castillo, C.J. (2025). Mitochondrial proteome basis for the biological variations in beef

color stability of *longissimus lumborum* muscle differing in ultimate pH and packaging methods. *Meat Science, 226*, 109842. https://doi.org/10.1016/j.meatsci.2025.109842

Li, J., Zhang, D., Tian, M., Li, X., Sun, X., Tang, Y., Hou, C., Wang, D., Min, C., & Qi, Y. (2025). Targeted control of beef spoilage: integrating slaughter-source tracking with packaging-temperature hurdles for precision preservation. *Food Research International, 224*, 117957. https://doi.org/10.1016/j.foodres.2025.117957

Liu, C., Wei, Q., Li, X., Han, D., Liu, J., Huang, F., & Zhang, C. (2022). Proteomic analyses of mitochondrial damage in postmortem beef muscles. *Journal of the Science of Food and Agriculture, 102*(10), 4182–4191. https://doi.org/10.1002/jsfa.11767

Lu, X., Wang, L., Shang, Y., Li, H., Qian, C., & Zhang, S. (2026). Progress on regulatory network and biomarker discovery of beef quality formation from a proteomics perspective. *Meat Research, 40*(8), 93–100 (in Chinese with English abstract). https://doi.org/10.7506/rlyj1001-8123-20260123-016

Luo, H., He, Y., Zhang, X., Ruan, Z., Luo, R., & Li, Y. (2021). Changes in postmortem energy metabolism of Qinchuan cattle meat during chilled storage and its effects on meat quality. *Food Science, 42*(17), 201–209 (in Chinese with English abstract). https://doi.org/10.7506/spkx1002-6630-20201013-112

Poirier, S., Coeuret, G., Champomier-Vergès, M.C., Desmonts, M.H., Werner, D., Feurer, C., Frémaux, B., Guillou, S., Luong, N.D.M., Rué, O., Loux, V., Zagorec, M., & Chaillou, S. (2023). Holistic integration of omics data reveals the drivers that shape the ecology of microbial meat spoilage scenarios. *Frontiers in Microbiology, 14*, 1286661. https://doi.org/10.3389/fmicb.2023.1286661

Ren, C., Bai, Y., Zhang, Y., Hou, C., Chen, L., Morton, J.D., Li, X., Wang, Z., & Zhang, D. (2025). Comprehensive study of protein phosphorylation, acetylation, ubiquitination and S-nitrosylation profiles in pre- and post-rigor meat. *Food Science and Human Wellness, 14*(6), 9250319. https://doi.org/10.26599/FSHW.2024.9250319

Shu, Y., Lv, J., Lou, A., Quan, W., & Shen, Q.W. (2025). Protein lysine acetylation regulates beef color stability during storage. *LWT, 220*, 117468. https://doi.org/10.1016/j.lwt.2025.117468

Subramanian, A., Tamayo, P., Mootha, V.K., Mukherjee, S., Ebert, B.L., Gillette, M.A., Paulovich, A., Pomeroy, S.L., Golub, T.R., Lander, E.S., & Mesirov, J.P. (2005). Gene set enrichment analysis: a knowledge-based approach for interpreting genome-wide expression profiles. *Proceedings of the National Academy of Sciences of the United States of America, 102*(43), 15545–15550. https://doi.org/10.1073/pnas.0506580102

Thamsborg, K.K.M., Lund, B.W., Byrne, D.V., Leisner, J.J., & Alexi, N. (2023). Cadaverine as a potential spoilage indicator in skin-packed beef and modified-atmosphere-packed beef. *Foods, 12*(24), 4489. https://doi.org/10.3390/foods12244489

Wang, X., Li, P., Chen, X., Cui, W., Ni, S., Xu, H., Xu, Y., Cai, K., Zhou, H., & Xu, B. (2025). Integrated microbiome and metabolomics analysis of spoilage characteristics of modified atmosphere packaged pork. *Food Research International, 203*, 115827. https://doi.org/10.1016/j.foodres.2025.115827

Xu, C., Wang, S., Bai, J., Chen, X., Shi, Y., Hao, J., & Zhao, B. (2024). Dynamic microbial community and metabolic profiling in refrigerated beef: insights from diverse packaging strategies. *Food Research International, 197*(Pt 1), 115170. https://doi.org/10.1016/j.foodres.2024.115170

Xu, H., Long, J., Ren, C., Jiang, L., Yu, B., Wang, Q., Zhao, Y., & Lei, L. (2027). Evaluation of combined ice-temperature and modified atmosphere packaging on preservation of Guizhou yellow beef and

development of a shelf-life prediction model. *Guizhou Agricultural Sciences*. In press (accepted 22 April 2026; publication scheduled for July 2027).

Yang, J., Yang, X., Liang, R., Zhu, L., Mao, Y., Dong, P., Hopkins, D.L., Luo, X., & Zhang, Y. (2022). The response of bacterial communities to carbon dioxide in high-oxygen modified atmosphere packaged beef steaks during chilled storage. *Food Research International, 151*, 110872. https://doi.org/10.1016/j.foodres.2021.110872

Yang, J., Chen, X., Duan, X., Li, K., Cheng, H., Sun, G., Luo, X., Hopkins, D.L., Holman, B.W.B., Zhang, Y., & Song, E. (2024). Investigation of oxygen packaging to maintain beef color stability and microbiology safety after periods of long-term superchilled storage. *Meat Science, 215*, 109548. https://doi.org/10.1016/j.meatsci.2024.109548

Yang, J., Yu, X., Liu, Y., Liang, R., Zhu, L., Dong, P., Zhang, Y., & Yang, X. (2025). The off-odor identification and CO_2-inhibition for high-oxygen packaged beef spoilage associated with *Brochothrix thermosphacta* growth and metabolism. *Food Research International, 216*, 116711. https://doi.org/10.1016/j.foodres.2025.116711

Yu, L., Pang, Y., Shen, G., Bai, B., Yang, Y., & Zeng, M. (2025). Identification and selection of volatile compounds derived from lipid oxidation as indicators for quality deterioration of frozen white meat and red meat using HS-SPME-GC-MS combined with OPLS-DA. *Food Chemistry, 463*(Pt 1), 141112. https://doi.org/10.1016/j.foodchem.2024.141112

Yuan, Y., Li, P., Li, J., Zhao, Q., Chang, Y., & He, X. (2024). Protein lipidation in health and disease: molecular basis, physiological function and pathological implication. *Signal Transduction and Targeted Therapy, 9*(1), 60. https://doi.org/10.1038/s41392-024-01759-7

Zhou, J., Zhao, Y., Jiang, L., Ran, J., Luo, W., Xu, H., Lei, L., Ai, R., Tan, J., & Yu, B. (2024). Characterization of biodiversity and meat quality in Guizhou yellow cattle: correlations among intrinsic factors. *Journal of Food Composition and Analysis, 132*, 106297. https://doi.org/10.1016/j.jfca.2024.106297

Zhu, Y., Gagaoua, M., Mullen, A.M., Kelly, A.L., Sweeney, T., Cafferky, J., Viala, D., & Hamill, R.M. (2021). A proteomic study for the discovery of beef tenderness biomarkers and prediction of Warner-Bratzler shear force measured on *Longissimus thoracis* muscles of young Limousin-sired bulls. *Foods, 10*(5), 952. https://doi.org/10.3390/foods10050952

Tables

Table 1. Conventional quality indicators of beef stored at −1 °C under 30% CO_2 / 20% O_2 / 50% N_2 (companion study, Xu et al., 2027). Values are mean ± SD (n = 3); different letters within a row indicate significant differences ($p < 0.05$).

Indicator	0 d	7 d	14 d
TVC (log CFU/g)	3.00 ± 0.10 ^{c}	3.53 ± 0.25 ^{b}	4.90 ± 0.10 ^{a}
TVB-N (mg/100 g)	10.38 ± 0.73 ^{c}	13.53 ± 1.13 ^{b}	16.29 ± 0.62 ^{a}
pH	6.00 ± 0.02 ^{a}	5.90 ± 0.04 ^{a}	5.50 ± 0.05 ^{b}
L*	30.45 ± 1.94 ^{a}	31.16 ± 0.36 ^{a}	29.60 ± 0.83 ^{a}
a*	21.59 ± 1.00 ^{a}	20.44 ± 0.30 ^{a}	16.71 ± 0.70 ^{b}

Sensory score (10-point)	8.80 ± 0.26 [a]	7.53 ± 0.21 [b]	6.53 ± 0.31 [c]

Figure legends

Figure 1. Protein and peptide identification. (A) Numbers of proteins and peptides identified in the nine samples; (B) distribution of peptide lengths in amino acids; (C) Venn diagram of proteins shared by and unique to groups A (0 d), B (7 d) and C (14 d).

Figure 2. Sample structure of the proteomic data. (A) PCA score plot; (B) OPLS-DA score plot (R^2X = 0.915, R^2Y = 0.982, Q^2 = 0.973).

Figure 3. Differentially abundant proteins (fold change > 1.5, $p < 0.05$). (A) Numbers of DAPs in the A vs B, A vs C and B vs C comparisons; (B–D) volcano plots for A vs B, A vs C and B vs C.

Figure 4. Functional enrichment of the A vs C comparison. (A) GO biological process and (B) GO cellular component terms; (C) KEGG pathways; (D, E) GSEA enrichment plots for oxidative phosphorylation and respiratory electron transport on the ranked protein list (normalised enrichment scores and FDR values are given in the panels).

Figure 5. Volatile organic compounds. (A) Venn diagram of the three groups; (B) total volatile concentration; (C) concentration of each chemical class; (D) proportion of each class; (E) aroma-attribute profile of the three groups on a 0–120 relative scale, derived from the odour descriptors of the identified volatiles (not panel data; section 2.5.3).

Figure 6. The dominant volatiles of (A) group A (0 d), (B) group B (7 d) and (C) group C (14 d).

Figure 7. Heatmap of the 11 volatile compounds that differed significantly among the three groups (one-way ANOVA, $p < 0.05$).

Figure 8. Distribution of 16S rRNA sequence lengths.

Figure 9. Alpha diversity of the bacterial community: Chao1, Simpson, Shannon, Pielou's evenness, observed species, Faith's PD and Good's coverage. Boxes show the median and interquartile range, whiskers extend to the most extreme values and points are individual samples; p values are from the Kruskal–Wallis test.

Figure 10. NMDS ordination of the bacterial community based on Bray–Curtis distances (stress < 0.2).

Figure 11. Relative abundance of the bacterial community at (A) phylum and (B) genus level.

Figure 12. Associations across the three omics layers. (A) DAP–volatile, (B) DAP–genus and (C) volatile–genus Pearson correlation matrices; (D) Mantel test results between matrices. Correlations were computed on the 0 d and 14 d samples only (n = 6, three replicates per time point; the 7 d samples were excluded because the volatile profile is non-monotonic at 7 d, see section 2.7). Dot size and colour intensity scale with the magnitude of r, red denotes positive and blue negative correlation, and one, two and three asterisks denote unadjusted $p < 0.05$, $p < 0.01$ and $p < 0.001$, respectively (at n = 6 these correspond to $|r| \geq 0.81$, 0.92 and 0.97). Because all variables were measured on the same two dates, the matrices are dominated by storage time (section 4.4).

Figures

Figure 1

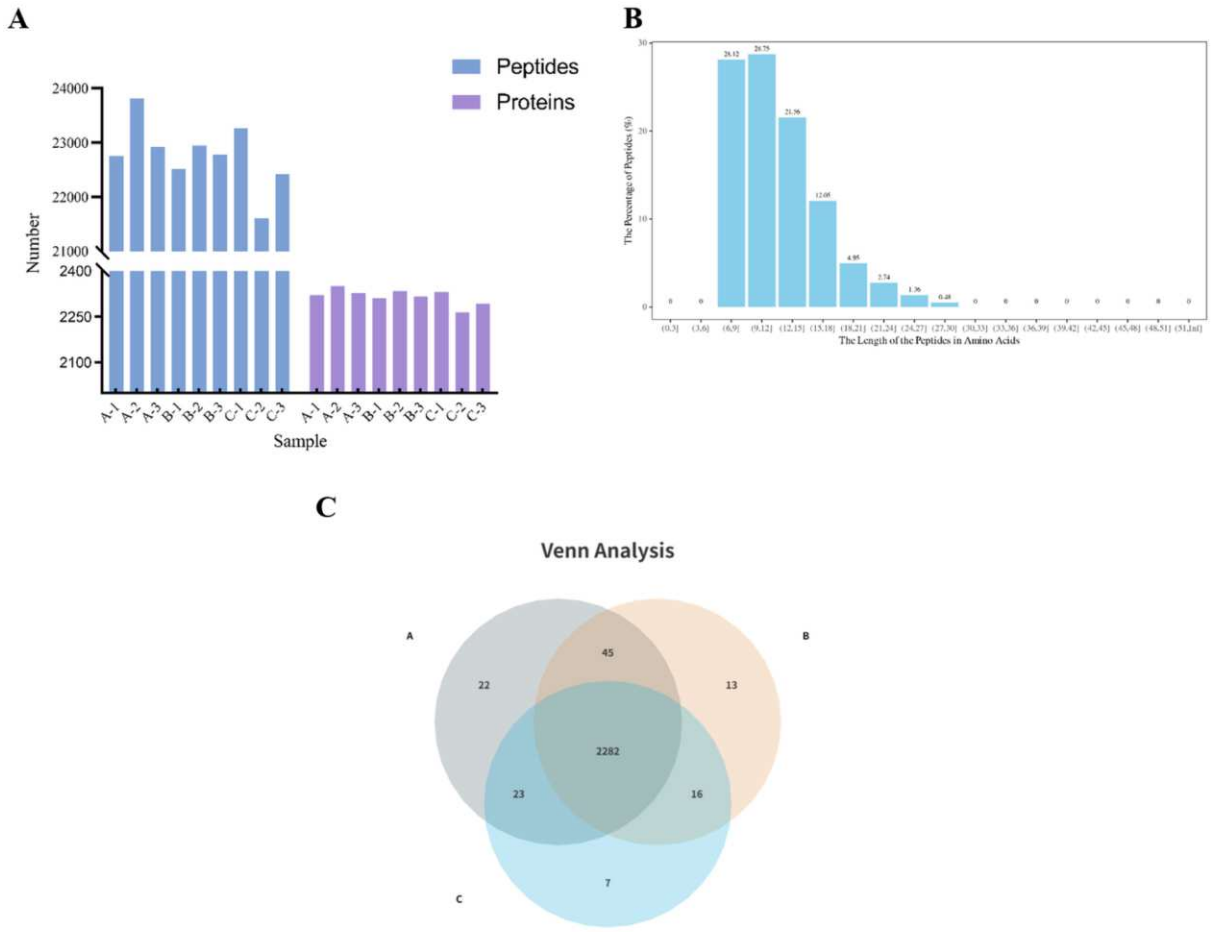

Figure 2

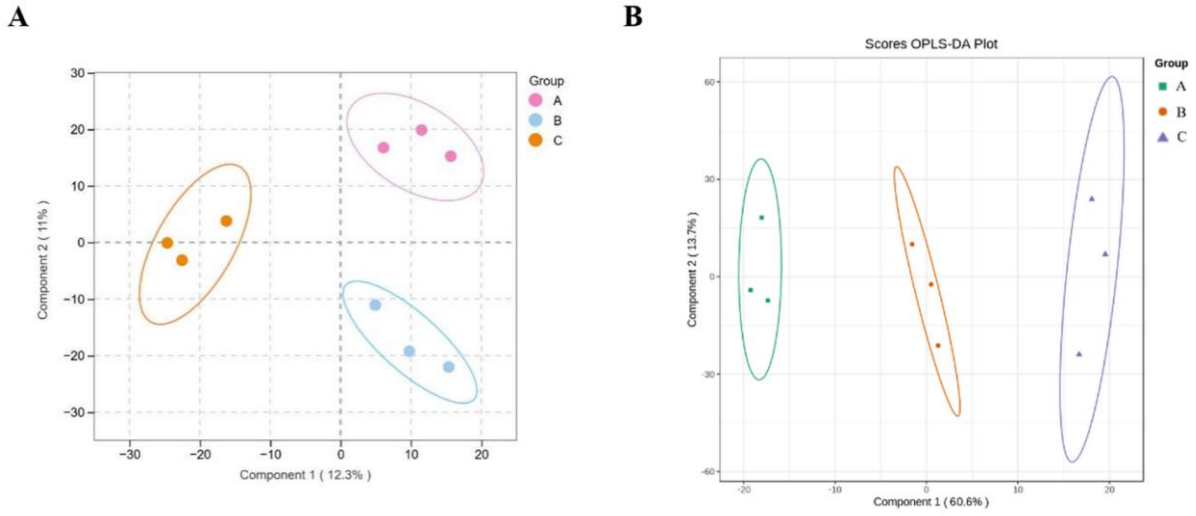

Figure 3

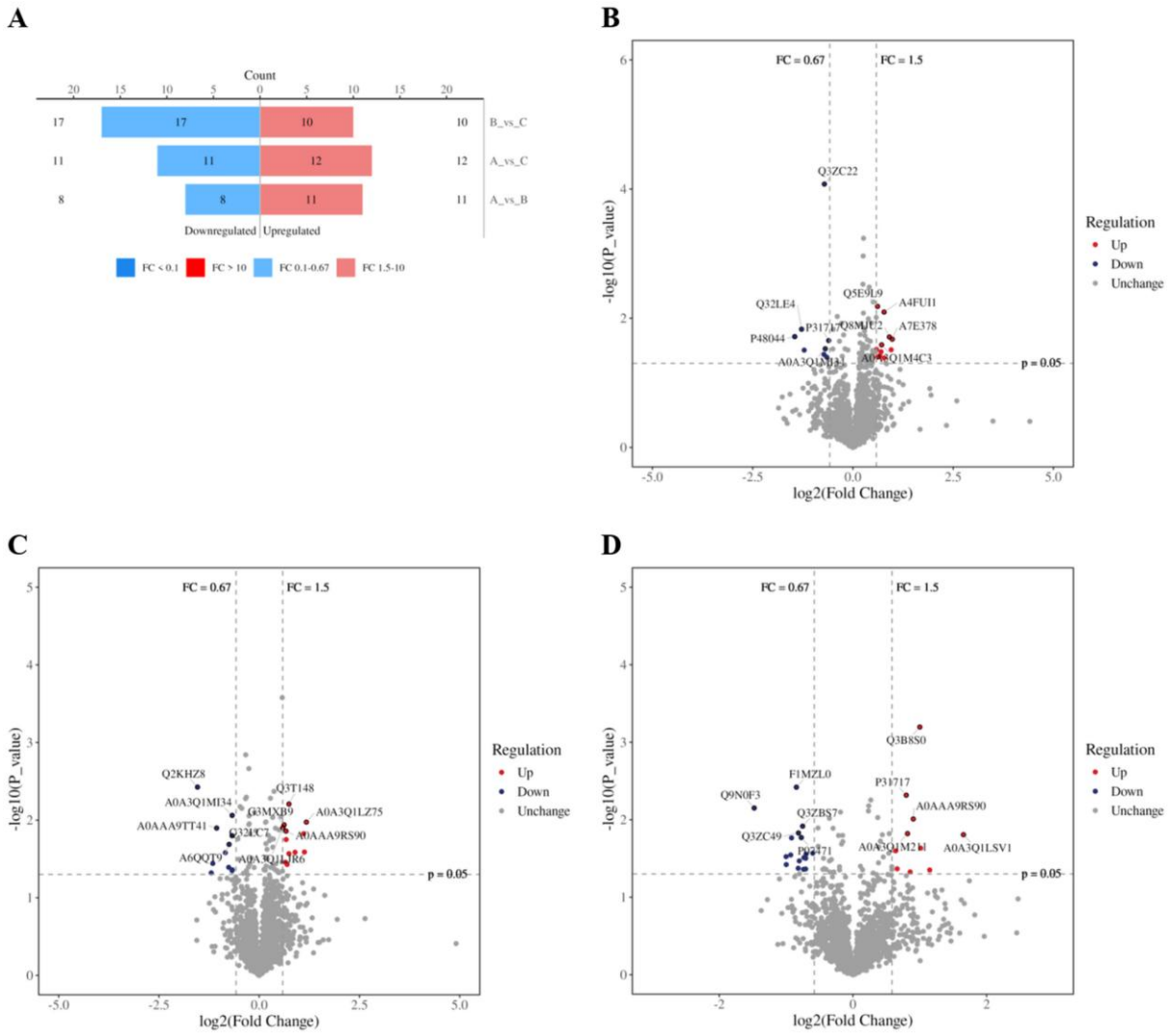
A
Count
20 15 10 5 0 5 10 15 20
17 17 10 10 B_vs_C
11 11 12 12 A_vs_C
8 8 11 11 A_vs_B
Downregulated Upregulated
FC < 0.1
FC > 10
FC 0.1-0.67
FC 1.5-10
B
FC = 0.67
FC = 1.5
p = 0.05
-log10(P_value)
log2(Fold Change)
Regulation
Up
Down
Unchange
Q3ZC22
Q5E9L9
A4FUI1
Q32LE4
P31717
Q8MUU2
A7E378
P48044
A0A3Q1M4C3
C
FC = 0.67
FC = 1.5
p = 0.05
-log10(P_value)
log2(Fold Change)
Regulation
Up
Down
Unchange
Q2KHZ8
Q3T148
A0A3Q1MI34
G3MXD9
A0A3Q1LZ75
A0AAA9TT41
Q32LC7
A0AAA9RS90
A6QQT9
D
FC = 0.67
FC = 1.5
p = 0.05
-log10(P_value)
log2(Fold Change)
Regulation
Up
Down
Unchange
Q3B8S0
F1MZL0
P31717
Q9N0F3
A0AAA9RS90
Q3ZBS7
Q3ZC49
A0A3Q1LSV1

Figure 4

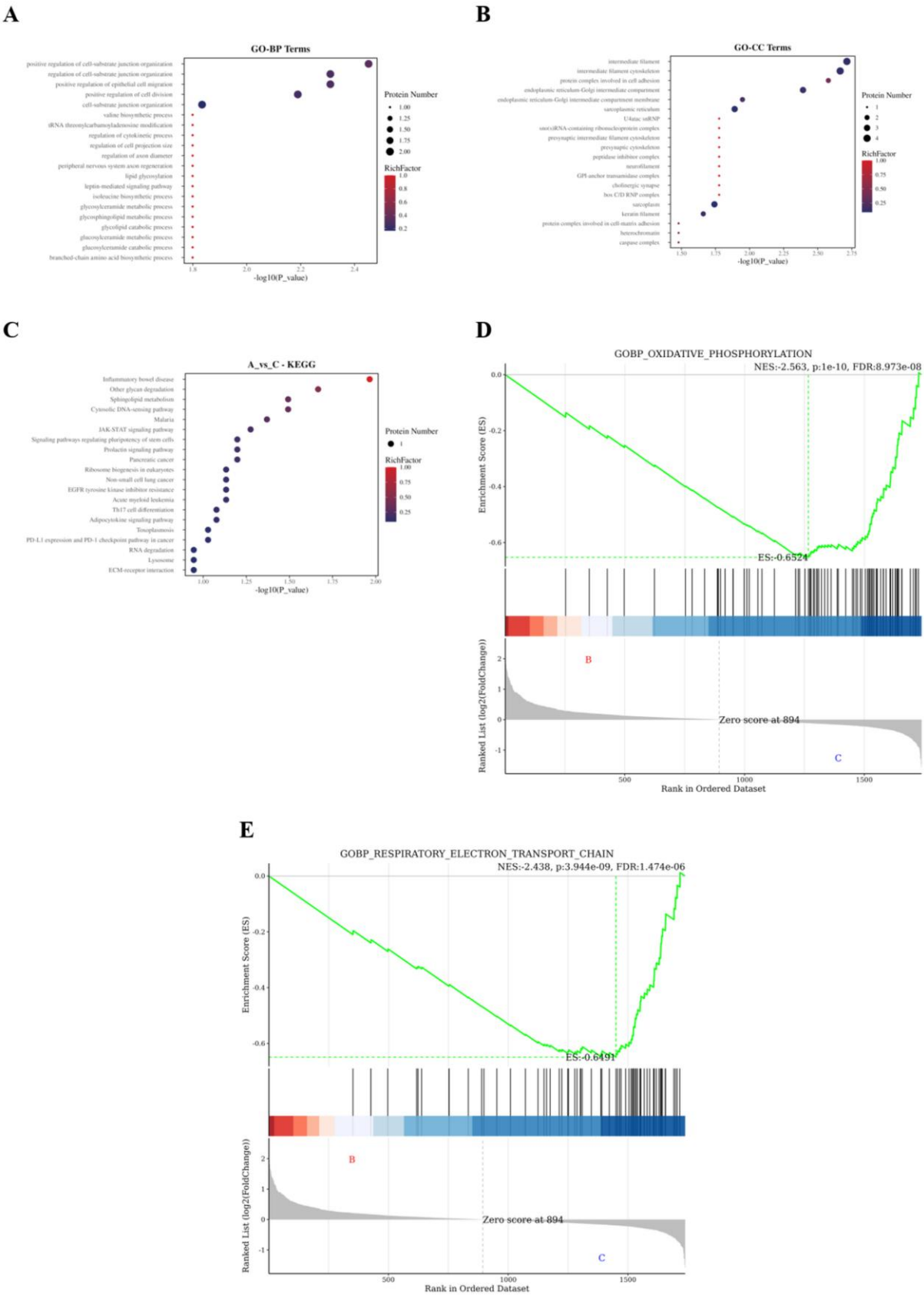
A
GO-BP Terms
positive regulation of cell-substrate junction organization
regulation of cell-substrate junction organization
positive regulation of epithelial cell migration
positive regulation of cell division
cell-substrate junction organization
valine biosynthetic process
tRNA threonylcarbamoyladenosine modification
regulation of cytokinetic process
regulation of cell projection size
regulation of axon diameter
peripheral nervous system axon regeneration
lipid glycosylation
leptin-mediated signaling pathway
isoleucine biosynthetic process
glycosylceramide metabolic process
glycosphingolipid metabolic process
glycolipid catabolic process
glucosylceramide metabolic process
glucosylceramide catabolic process
branched-chain amino acid biosynthetic process
1.8
2.0
2.2
2.4
-log10(P_value)
Protein Number
1.00
1.25
1.50
1.75
2.00
RichFactor
1.0
0.8
0.6
0.4
0.2
B
GO-CC Terms
intermediate filament
intermediate filament cytoskeleton
protein complex involved in cell adhesion
endoplasmic reticulum-Golgi intermediate compartment
endoplasmic reticulum-Golgi intermediate compartment membrane
sarcoplasmic reticulum
U4/atac snRNP
snoRNA-containing ribonucleoprotein complex
presynaptic intermediate filament cytoskeleton
presynaptic cytoskeleton
peptidase inhibitor complex
neurofilament
GPI-anchor transamidase complex
cholinergic synapse
box C/D RNP complex
sarcoplasm
keratin filament
protein complex involved in cell-matrix adhesion
heterochromatin
caspase complex
1.50
1.75
2.00
2.25
2.50
2.75
-log10(P_value)
Protein Number
1
2
3
4
RichFactor
1.00
0.75
0.50
0.25
C
A_vs_C - KEGG
Inflammatory bowel disease
Other glycan degradation
Sphingolipid metabolism
Cytosolic DNA-sensing pathway
Malaria
JAK-STAT signaling pathway
Signaling pathways regulating pluripotency of stem cells
Prolactin signaling pathway
Pancreatic cancer
Ribosome biogenesis in eukaryotes
Non-small cell lung cancer
EGFR tyrosine kinase inhibitor resistance
Acute myeloid leukemia
Th17 cell differentiation
Adipocytokine signaling pathway
Toxoplasmosis
PD-L1 expression and PD-1 checkpoint pathway in cancer
RNA degradation
Lysosome
ECM-receptor interaction
1.00
1.25
1.50
1.75
2.00
-log10(P_value)
Protein Number
1
RichFactor
1.00
0.75
0.50
0.25
D
GOBP_OXIDATIVE_PHOSPHORYLATION
NES:-2.563, p:1e-10, FDR:8.973e-08
Enrichment Score (ES)
0.0
-0.2
-0.4
-0.6
ES:-0.6524
B
Ranked List (log2(FoldChange))
2
1
0
-1
Zero score at 894
C
500
1000
1500
Rank in Ordered Dataset
E
GOBP_RESPIRATORY_ELECTRON_TRANSPORT_CHAIN
NES:-2.438, p:3.944e-09, FDR:1.474e-06
Enrichment Score (ES)
0.0
-0.2
-0.4
-0.6
ES:-0.6491
B
Ranked List (log2(FoldChange))
2
1
0
-1
Zero score at 894
C
500
1000
1500
Rank in Ordered Dataset

Figure 5

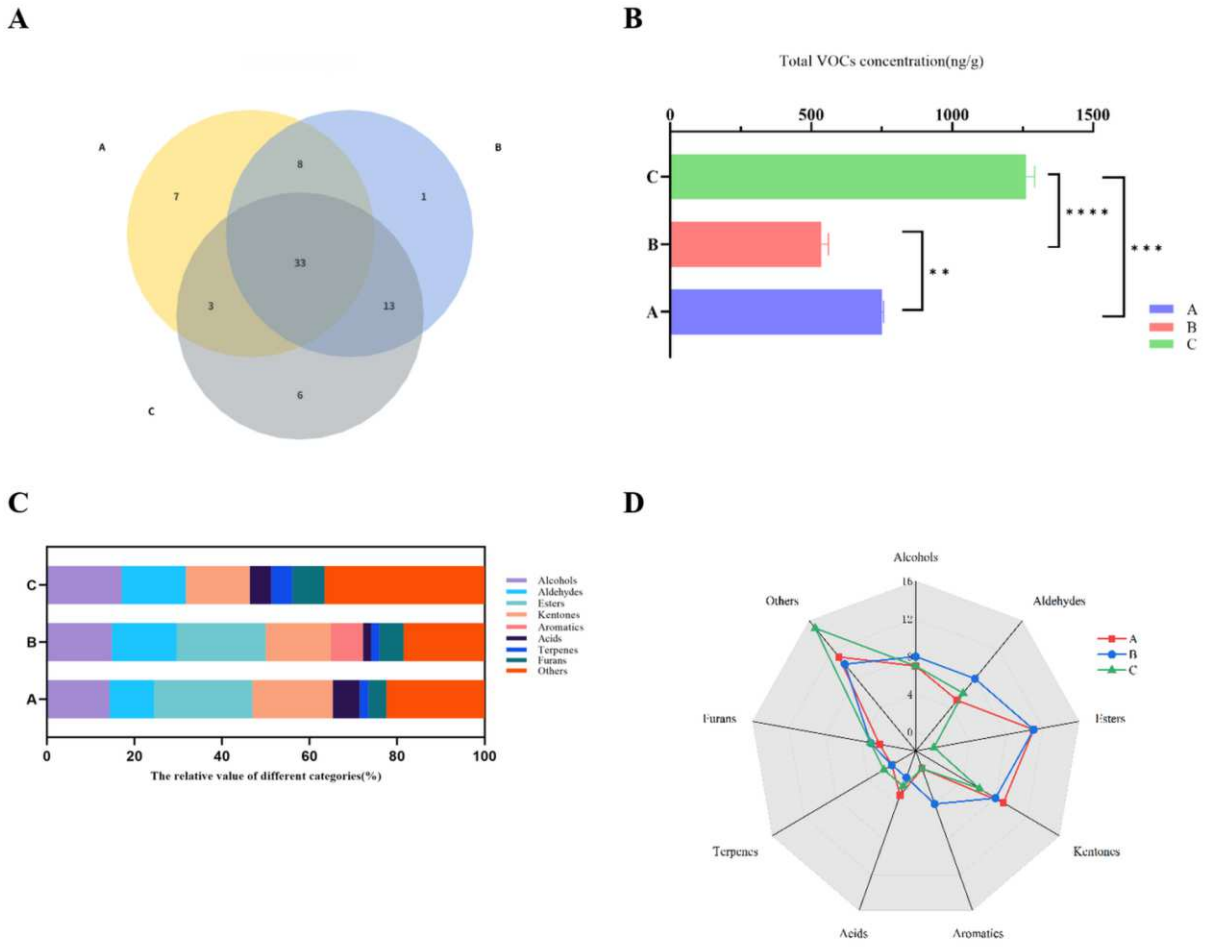

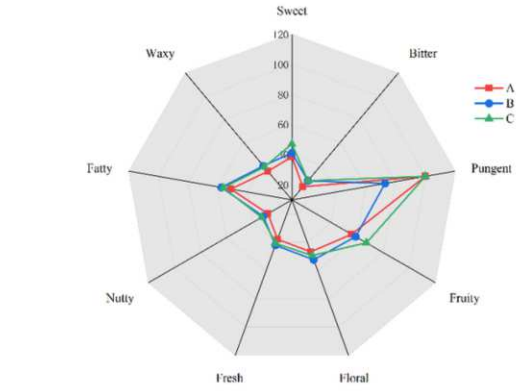

Figure 6

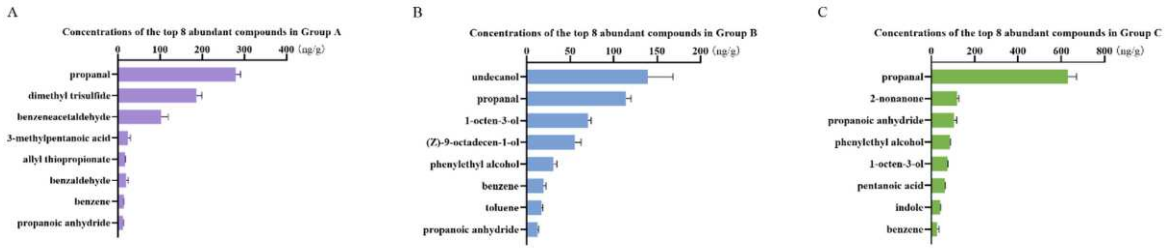

Figure 7

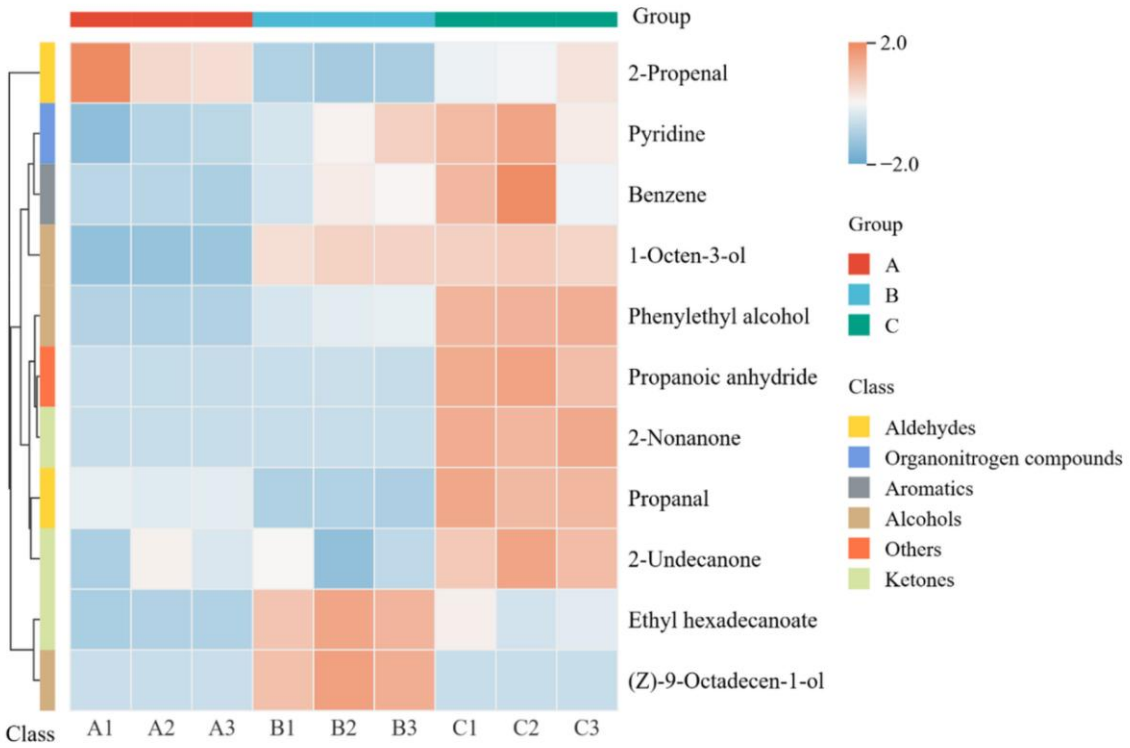

Figure 8

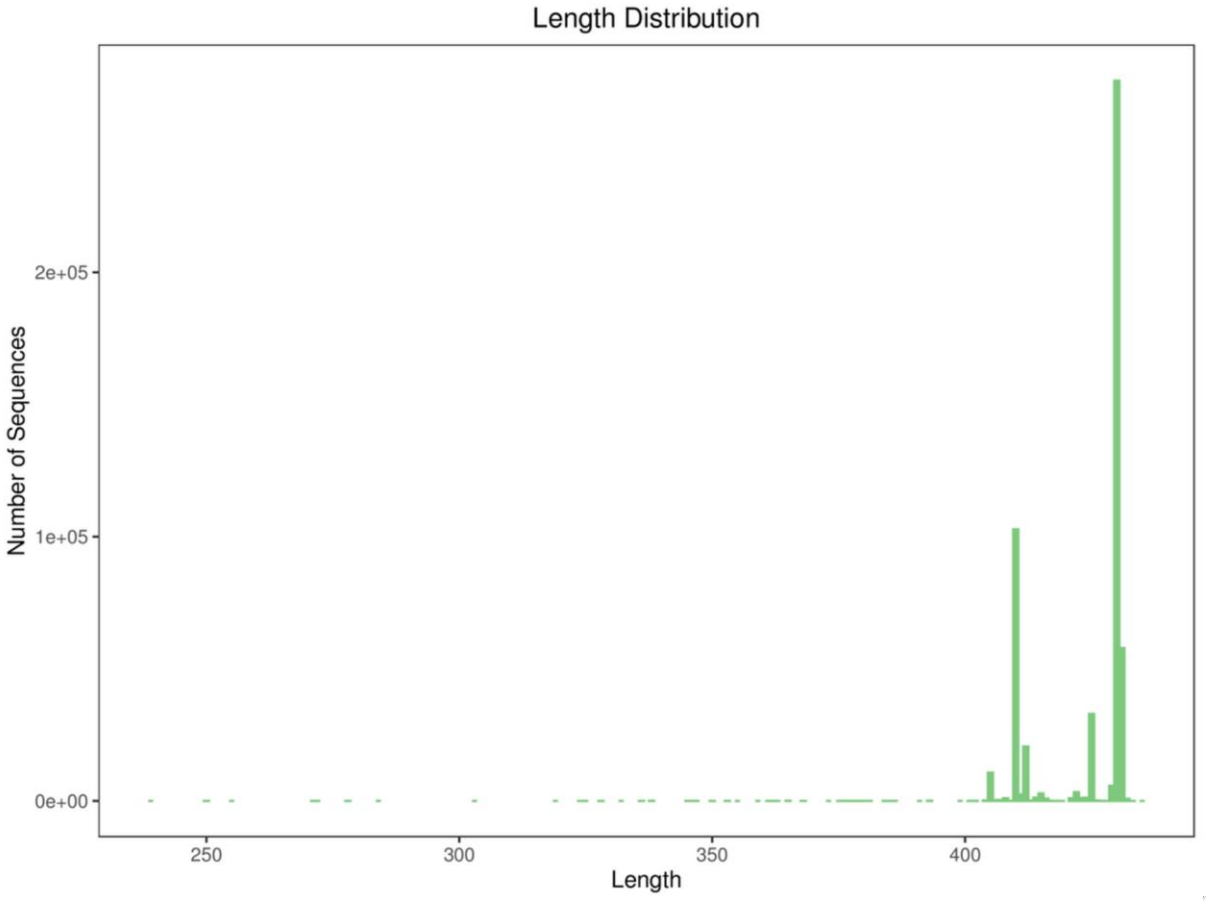
Length Distribution
Number of Sequences
2e+05
1e+05
0e+00
250
300
350
400
Length

Figure 9

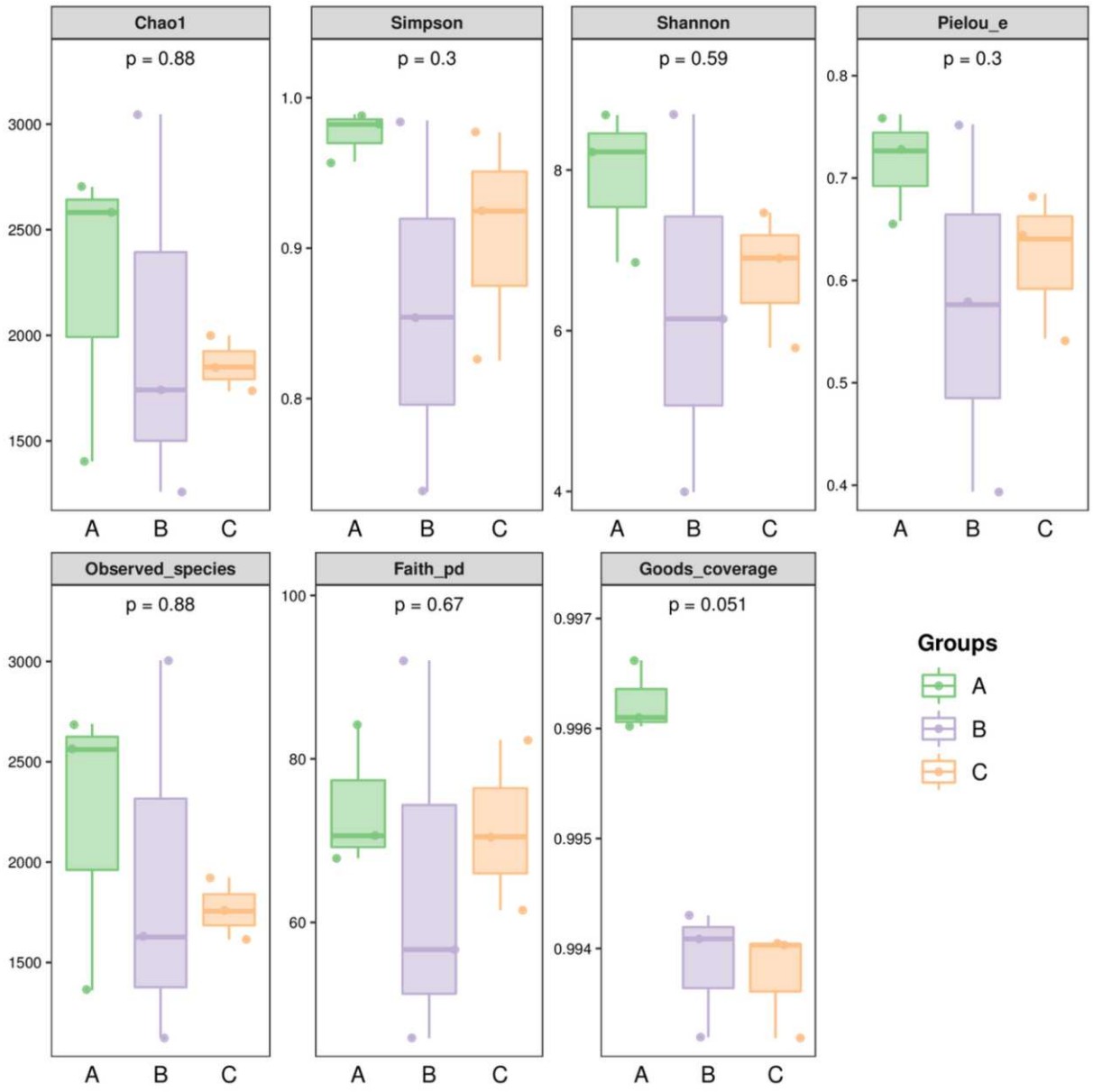
Chao1
p = 0.88
3000
2500
2000
1500
A
B
C
Simpson
p = 0.3
1.0
0.9
0.8
A
B
C
Shannon
p = 0.59
8
6
4
A
B
C
Pielou_e
p = 0.3
0.8
0.7
0.6
0.5
0.4
A
B
C
Observed_species
p = 0.88
3000
2500
2000
1500
A
B
C
Faith_pd
p = 0.67
100
80
60
A
B
C
Goods_coverage
p = 0.051
0.997
0.996
0.995
0.994
A
B
C
Groups
A
B
C

Figure 10

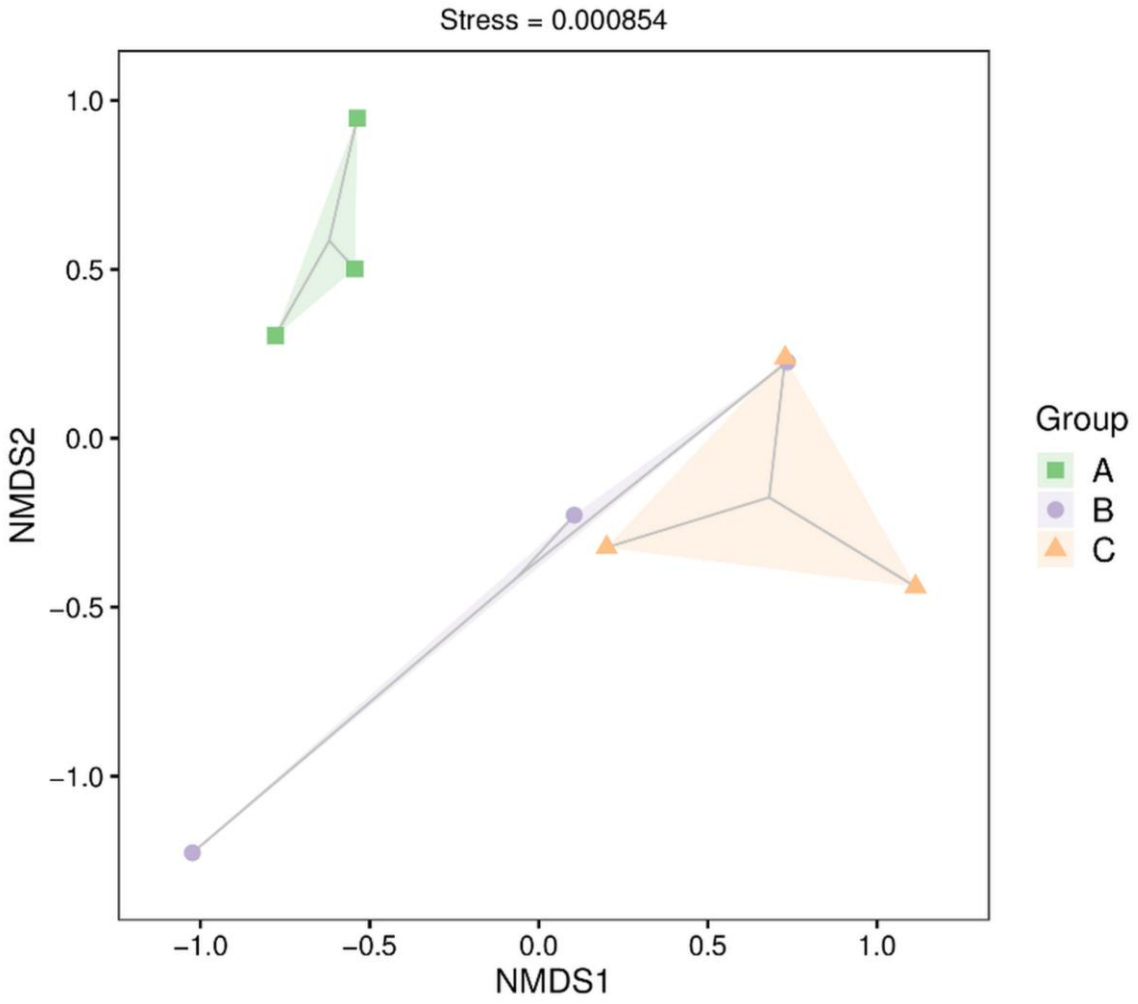

Figure 11

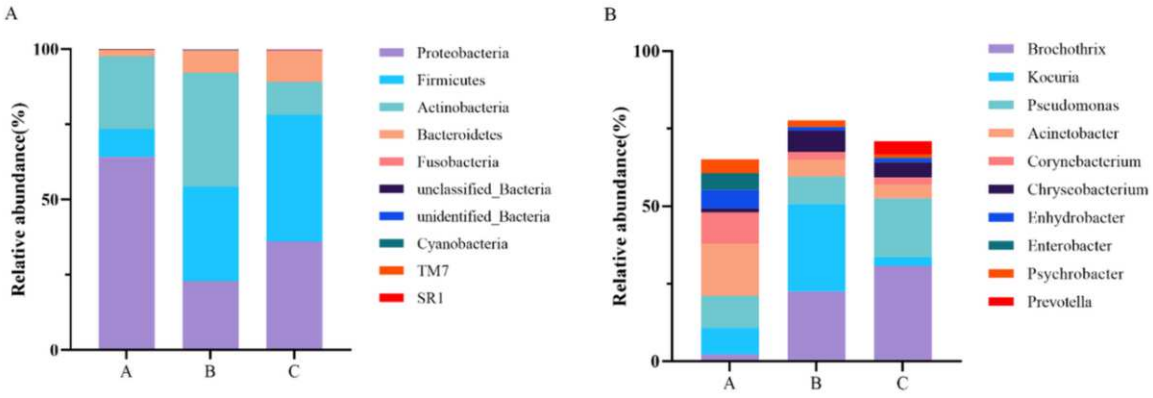

Figure 12

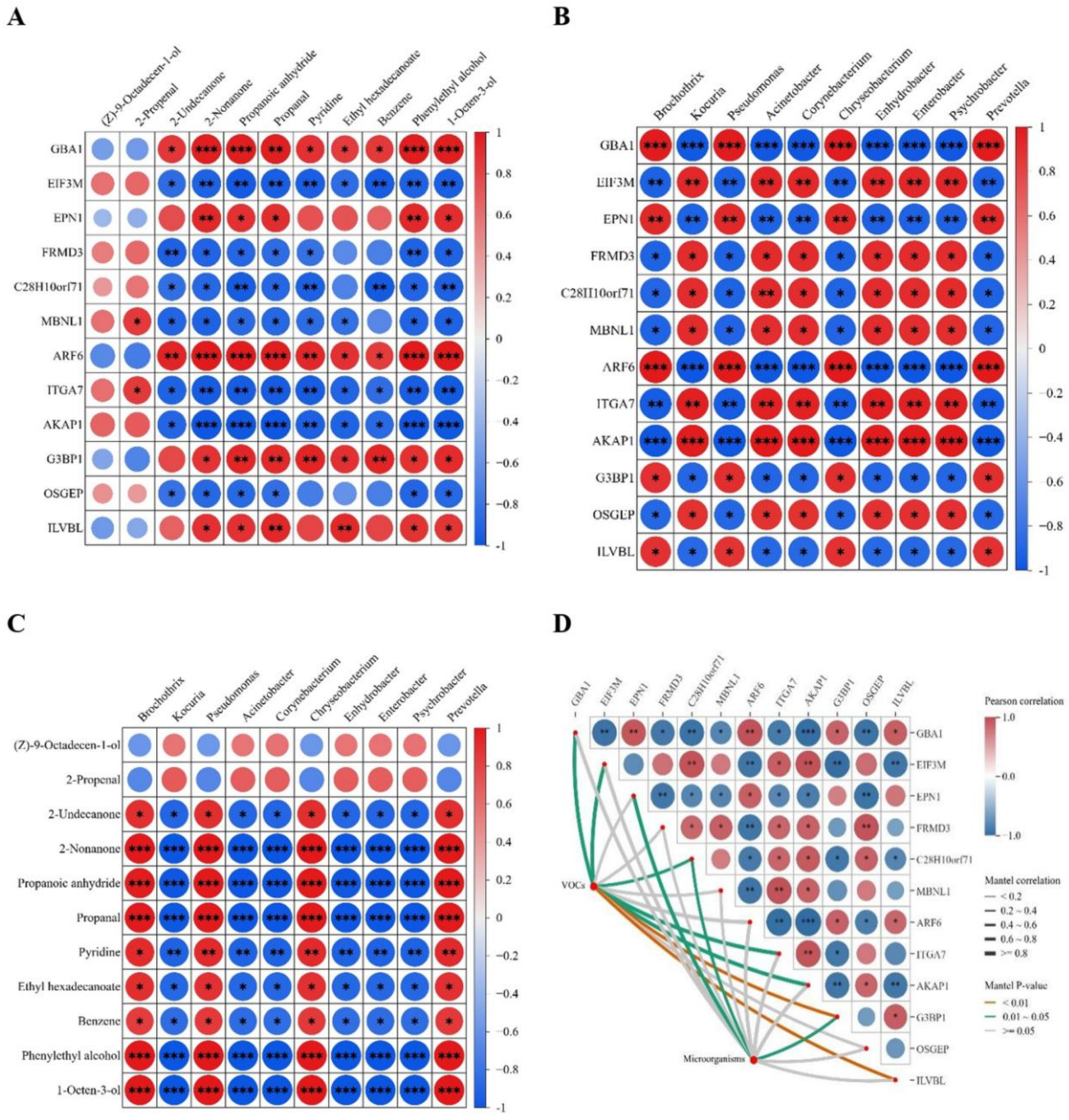
A
(Z)-9-Octadecen-1-ol
2-Propenal
2-Undecanone
2-Nonanone
Propanoic anhydride
Propanal
Pyridine
Ethyl hexadecanoate
Benzene
Phenylethyl alcohol
1-Octen-3-ol
GBA1
EIF3M
EPN1
FRMD3
C28H10orf71
MBNL1
ARF6
ITGA7
AKAP1
G3BP1
OSGEP
ILVBL
1
0.8
0.6
0.4
0.2
0
−0.2
−0.4
−0.6
−0.8
-1
B
Brochothrix
Kocuria
Pseudomonas
Acinetobacter
Corynebacterium
Chryseobacterium
Enhydrobacter
Enterobacter
Psychrobacter
Prevotella
GBA1
EIF3M
EPN1
FRMD3
C28H10orf71
MBNL1
ARF6
ITGA7
AKAP1
G3BP1
OSGEP
ILVBL
1
0.8
0.6
0.4
0.2
0
−0.2
−0.4
−0.6
−0.8
-1
C
Brochothrix
Kocuria
Pseudomonas
Acinetobacter
Corynebacterium
Chryseobacterium
Enhydrobacter
Enterobacter
Psychrobacter
Prevotella
(Z)-9-Octadecen-1-ol
2-Propenal
2-Undecanone
2-Nonanone
Propanoic anhydride
Propanal
Pyridine
Ethyl hexadecanoate
Benzene
Phenylethyl alcohol
1-Octen-3-ol
1
0.8
0.6
0.4
0.2
0
−0.2
−0.4
−0.6
−0.8
-1
D
GBA1
EIF3M
EPN1
FRMD3
C28H10orf71
MBNL1
ARF6
ITGA7
AKAP1
G3BP1
OSGEP
ILVBL
VOCs
Microorganisms
Pearson correlation
1.0
0.0
−1.0
Mantel correlation
< 0.2
0.2 ~ 0.4
0.4 ~ 0.6
0.6 ~ 0.8
>= 0.8
Mantel P-value
< 0.01
0.01 ~ 0.05
>= 0.05